Predicting the deflection and sub-surface stress field within two-dimensional inhomogeneously elastic bonded layered solids...

Article *in* International Journal of Solids and Structures · November 2011

DOI: 10.1016/j.ijsolstr.2011.07.017

CITATIONS
11

READS
21

3 authors:

S. J. Chidlow
Liverpool John Moores University
15 PUBLICATIONS **44** CITATIONS
SEE PROFILE

M. Teodorescu
University of California, Santa Cruz
57 PUBLICATIONS **464** CITATIONS
SEE PROFILE

Nicholas D. Vaughan
Cranfield University
73 PUBLICATIONS **758** CITATIONS
SEE PROFILE

Predicting the deflection and sub-surface stress field within two-dimensional inhomogeneously elastic bonded layered solids under pressure

S. J. Chidlow*, M. Teodorescu[1]*+, N.D. Vaughan*

*Department of Automotive Engineering, School of Engineering, Cranfield University, Cranfield, MK43 0AL, UK
+Baskin School of Engineering, University of California at Santa Cruz, Santa Cruz, CA USA

Abstract

This paper describes a Fourier series based solution method for the displacements and sub-surface stresses within a graded elastic layered solid under pressure. The solid is assumed to be in a state of plane strain and thus the derived solution is valid for two-dimensional problems. Whilst this method provides a fully analytic solution when the contact pressure is known exactly, it may also be used when the contact pressure is only known numerically (see section 4). The solution given in this paper is generic and easily utilised to solve real problems as it requires only known physical characteristics of the solid under study and an applied surface pressure.

The solid consists of two distinct regions which are considered to be perfectly bonded. These comprise a graded elastic coating whose shear modulus varies exponentially with the depth coordinate and a homogeneously elastic substrate. As the stresses and displacements induced by the applied pressure decay very quickly outside of the contact region, the contact problem need only be solved in a small piece of the solid as the remainder is unaffected. It is found that accurate results are obtained when the contact problem is solved over a region of the solid ten times larger

[1]*Corresponding author's email address : m.s.teodorescu@cranfield.ac.uk*

than the contact region. This method as a result is computationally cheap to use as the number of Fourier modes needed to accurately capture the solution is small.

Keywords: Contact mechanics, Layered solids, Graded elasticity coatings, Functionally graded materials

1. Introduction

Protective coatings are often used in engineering applications where motion and force is transmitted through direct contact. These coatings are usually deposited over a base material and may consist of one or more layers whose mechanical properties (e.g. hard or soft, thick or thin) are carefully tailored for the intended purpose and environment they must operate in. Finding the ideal coating requires a good understanding of the physical context of the application as well as the mechanical properties of both the coating and substrate.

Often, the mechanical properties of these coatings are far from homogeneous. It is common to see either a transition zone where the mechanical properties of the layer progressively morph into the ones of the substrate (e.g. Shulha et al., 2004) or coatings that are engineered in such a way that their properties continuously change throughout their thickness (Uozato et al., 2005; Barbezat, 2008). The latter materials are usually termed functionally graded (FGMs) and are a relatively new concept in material design (Suresh et al., 1999, 1998).

Existing models that seek to approximate the contact problem involving FGMs tend to assume that the material is split into two distinct regions corresponding to the coating and substrate. The modulus of elasticity within the coating is assumed to depend on the depth coordinate in some pre-

determined way whilst the substrate is assumed to be homogeneous. Common approximations let the modulus of elasticity within the coating follow either a simple power law (e.g. Giannakopoulos and Suresh, 1997) or an exponential variation (e.g. Guler and Erdogan, 2004).

Attempts to model the contact problem involving inhomogeneous materials have proved difficult as the fully three-dimensional problem tends to be resistant to analytical approaches. Giannakopoulos and Suresh, 1997 presented some simple analytical models for the determination of the stresses and displacement within an inhomogeneous three-dimensional medium subject to a point force using both power law and exponential variations of the modulus of elasticity. The model solutions produced were then compared to numerical solutions obtained using the finite element method. A numerical method based on the Fast Fourier Transform (FFT) was proposed by Wang et al., 2010 to investigate partial slip contacts again in a three-dimensional context, however these authors give no clear picture how the elasticity within the coating is modelled. Zhong and Shang, 2008 detail an analytic solution for the stresses and displacements present in three-dimensional functionally graded plates of finite depth. Their solution comprises a double Fourier series in the horizontal variables and is valid for shear moduli following both the power law and exponential variations but the pressure distributions considered are specially chosen so that the solutions of the stresses and displacements comprise of only a single Fourier mode and are thus limited.

Instead of solving the fully three dimensional contact problem, the plane strain/plane stress assumption can be invoked in some cases. The resulting two-dimensional problem is simpler to study and has the advantage of reducing the number of equations that must be solved to fully determine the stress field and deflections induced by the contact. Sadd, 2010 presents some simple solutions

for the stresses and displacements within an inhomogeneous solid using an Airy stress function. These solutions tend to be somewhat limited as the stress functions considered are in general considered to satisfy the biharmonic equation which is not true in the majority of problems involving inhomogeneous media. Teodorescu et al., 2009; Teodorescu and Rahnejat, 2007 solve the contact problem using Fourier series decomposition and present an iterative algorithm for determining the contact footprint resulting from a rigid indenter. This method has the advantage that all quantities appearing in the solution may be evaluated analytically but the layers comprising the solid are taken to be homogeneous which is often not the case. Guler and Erdogan, 2004 and Ke and Wang, 2007 take the alternate approach of solving the contact problem using Fourier transform methods. These methods do in theory solve the contact problem exactly but typically determination of the integrals appearing in the solution can only be achieved using numerical methods. Chidlow et al., 2010 presented analytical solutions for the sub-surface stresses and deflection induced by pressure functions applied normally to the surface of semi-infinite graded elastic solids. Under the assumption that the stresses and displacements induced by contact pressure die very quickly outside of the contact, they formulated the contact problem in terms of an Airy stress function which was solved in a small region of the solid. The solution presented within this work was found to be computationally cheap to apply but was limited by the assumptions made about the modulus of elasticity to solids that become increasingly stiff below their surface.

The model presented in this paper builds on the work of Teodorescu et al., 2009 and Chidlow et al., 2011 to solve for the stresses and deflections resulting from the contact problem in graded elastic bonded layered solids. The modulus of elasticity within the coating is assumed to vary

exponentially with the depth coordinate whilst the substrate is considered to be homogeneously elastic. The knowledge that outside of the contact region the stresses and deflections induced by the applied surface pressure decay very quickly is used to show how the contact problem may be solved only in a small part of the solid rather than the solid as a whole. Unlike the previous investigation by Chidlow et al., 2010, the contact problem solved in this work is formulated in terms of the displacements within the problem. This has the advantage that the underlying matching conditions between the coating and substrate which ensure perfect bonding are more easily dealt with.

The layout of this paper is as follows. In Section 2, we describe the mathematical formulation of the contact problem whilst in Section 3 we describe the solution method used to analytically determine the sub-surface stresses and deflection and consider some special limiting cases in which the solution may be simplified. In Section 4 we discuss some of the practical issues that need to be considered when using this solution method and produce numerical results using our model in Section 5. This paper concludes with a summary of our findings in Section 6.

2. Formulation of the problem

This work predicts the subsurface stresses and deformation of a linearly elastic inhomogeneous bonded layered solid loaded by a pressure acting normally to the solid surface. A cartesian coordinate system in the (x,y) plane is used to describe the position of the solid with the y-axis directed positively upwards.

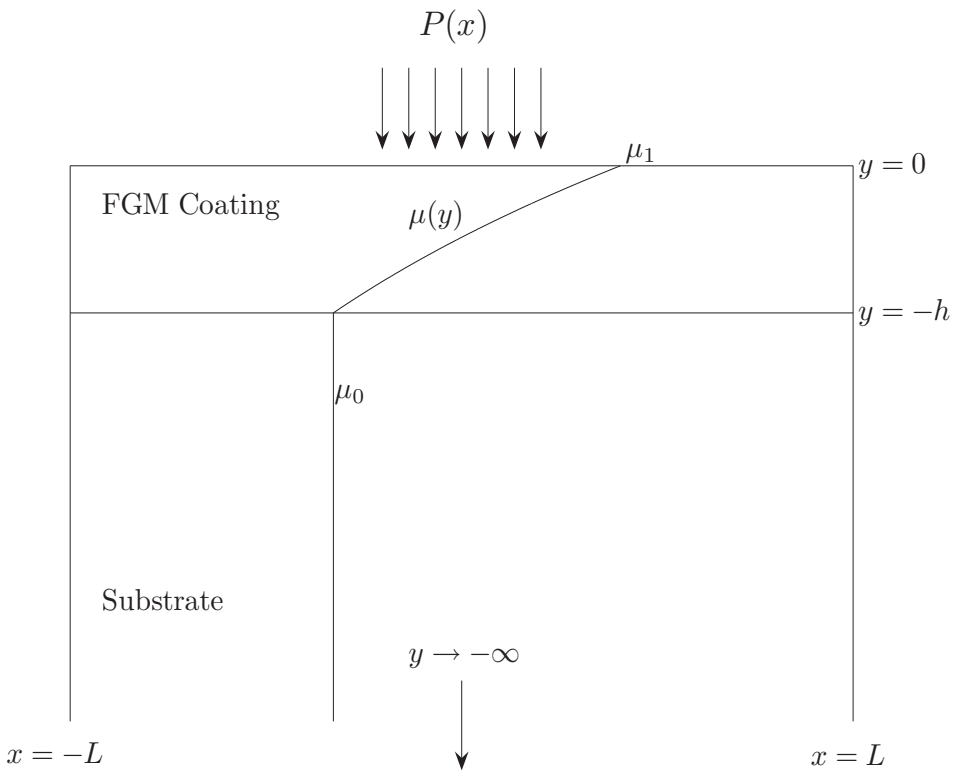

Figure 1: A definition sketch of the problem.

The solid under study is considered in a state of plane strain, occupies $-L \leq x \leq L, -\infty < y \leq 0$ and is split in two distinct regions. The upper region $-L \leq x \leq L, -h \leq y \leq 0$ represents an inhomogeneously elastic coating with a shear modulus that varies with the vertical coordinate but is assumed locally isotropic in the horizontal direction, whilst the lower region $-L \leq x \leq L, -\infty < y < -h$ represents a homogeneous elastic substrate. The shear modulus within the solid

is represented as

$$\mu(y) = \begin{cases} \mu_1 e^{\alpha y}, & -h \leq y \leq 0, \\ \mu_0, & -\infty < y < -h \end{cases} \tag{1}$$

It is assumed here that the shear modulus is continuous across the interface between the two layers and thus a simple calculation gives $\mu_1 = \mu_0 e^{\alpha h}$. The Poisson ratio denoted ν is assumed constant and equivalent in both the coating and the substrate.

The governing equations in this problem are the equilibrium equations in the absence of body forces which are stated below in terms of the stresses present in the solid for brevity (see for example Timoshenko and Goodier, 1961).

$$\frac{\partial \sigma_{xx}}{\partial x} + \frac{\partial \sigma_{xy}}{\partial y} = 0, \tag{2a}$$

$$\frac{\partial \sigma_{xy}}{\partial x} + \frac{\partial \sigma_{yy}}{\partial y} = 0. \tag{2b}$$

As the pressure force is applied normally to the solid surface, the boundary conditions applied on the solid surface are:

$$\begin{aligned} \sigma_{yy}(x,0) &= -P(x), \\ \sigma_{xy}(x,0) &= 0, \end{aligned} \tag{3}$$

are applied which specify a frictionless contact. The pressure function in this problem is of the form

$$P(x) = \begin{cases} p(x) & |x| \leq a, \\ 0 & |x| \geq a, \end{cases} \tag{4}$$

so that the pressure is non-zero only in some small interval $(-a,a)$ where a is referred to as the contact radius.

The boundaries $x = \pm L$ are deemed to represent the distance at which the applied pressure force ceases to effect the solid and thus we stipulate that

$$\sigma_{xx}(-L,y) = v(-L,y) = 0,$$
$$\sigma_{xx}(L,y) = v(L,y) = 0, \tag{5}$$

so that both the horizontal stresses and vertical displacement vanish. A discussion of how to determine an appropriate choice of L is conducted in section 5.1.

In addition to the boundary conditions already applied, we stipulate that the displacements u and v remain bounded everywhere. The application of the radiation conditions

$$u(x,-\infty), v(x,-\infty) \to 0 \tag{6}$$

ensure that the displacements decay far below the solid surface.

It should be noted that matching conditions across the interface $y = -h$ are required to uniquely determine the solution of the problem. As the coating and substrate are considered to be perfectly bonded, the conditions

$$\sigma_{yy}^{(c)} = \sigma_{yy}^{(s)}, \tag{7a}$$
$$\sigma_{xy}^{(c)} = \sigma_{xy}^{(s)}, \tag{7b}$$
$$u^{(c)} = u^{(s)}, \tag{7c}$$
$$v^{(c)} = v^{(s)}, \tag{7d}$$

which represent continuity of stress and displacement across the interface are applied.

The contact problem under study is now fully specified. However, it will be convenient to non-dimensionalise the independent variables x and y and solve an equivalent dimensionless problem. With this in mind, we introduce the variables $x = aX$, $y = aY$ which corresponds to non-dimensionalising the independent variables with respect to the contact radius a and note that

$$\frac{\partial}{\partial x} = \frac{\partial}{\partial X}\frac{\mathrm{d}X}{\mathrm{d}x} = \frac{1}{a}\frac{\partial}{\partial X}, \tag{8a}$$

$$\frac{\partial}{\partial y} = \frac{\partial}{\partial Y}\frac{\mathrm{d}Y}{\mathrm{d}y} = \frac{1}{a}\frac{\partial}{\partial Y}. \tag{8b}$$

Our aim in this paper is to solve the contact problem in terms of the dimensionless displacements u and v. However, before we can do this, we need to re-write the equations of equilibrium in terms of the dimensionless displacements $u(X,Y)$ and $v(X,Y)$. It may be easily verified from Hooke's law that

$$\sigma_{xx} = \frac{2\mu(Y)}{a(1-2\nu)}\left((1-\nu)\frac{\partial u}{\partial X} + \nu\frac{\partial v}{\partial Y}\right), \tag{9a}$$

$$\sigma_{yy} = \frac{2\mu(Y)}{a(1-2\nu)}\left((1-\nu)\frac{\partial v}{\partial Y} + \nu\frac{\partial u}{\partial X}\right), \tag{9b}$$

$$\sigma_{xy} = \frac{\mu(Y)}{a}\left(\frac{\partial u}{\partial Y} + \frac{\partial v}{\partial X}\right). \tag{9c}$$

Substituting equations (9a)-(9c) into (2a) and (2b) yields the coupled system

$$\frac{\partial}{\partial X}\left(\frac{2\mu(Y)}{1-2\nu}\left\{(1-\nu)\frac{\partial u}{\partial X} + \nu\frac{\partial v}{\partial Y}\right\}\right) + \frac{\partial}{\partial Y}\left(\mu(Y)\left\{\frac{\partial u}{\partial Y} + \frac{\partial v}{\partial X}\right\}\right) = 0, \tag{10}$$

$$\frac{\partial}{\partial X}\left(\mu(Y)\left\{\frac{\partial u}{\partial Y} + \frac{\partial v}{\partial X}\right\}\right) + \frac{\partial}{\partial Y}\left(\frac{2\mu(Y)}{1-2\nu}\left\{\nu\frac{\partial u}{\partial X} + (1-\nu)\frac{\partial v}{\partial Y}\right\}\right) = 0, \tag{11}$$

which are the equilibrium equations written in terms of the displacements. These equations take

different forms in each layer. It may be seen that in the coating

$$2(1-\nu)\frac{\partial^2 u^{(c)}}{\partial X^2}+(1-2\nu)\frac{\partial^2 u^{(c)}}{\partial Y^2}+\frac{\partial^2 v^{(c)}}{\partial X\partial Y}+\hat{\alpha}(1-2\nu)\frac{\partial u^{(c)}}{\partial Y}+\hat{\alpha}(1-2\nu)\frac{\partial v^{(c)}}{\partial X}=0, \tag{12a}$$

$$(1-2\nu)\frac{\partial^2 v^{(c)}}{\partial X^2}+2(1-\nu)\frac{\partial^2 v^{(c)}}{\partial Y^2}+\frac{\partial^2 u^{(c)}}{\partial X\partial Y}+2\hat{\alpha}\nu\frac{\partial u^{(c)}}{\partial X}+2\hat{\alpha}(1-\nu)\frac{\partial v^{(c)}}{\partial Y}=0, \tag{12b}$$

which hold for $-\hat{L}\leq X\leq\hat{L}, -\hat{h}\leq Y\leq 0$, whilst in the substrate

$$2(1-\nu)\frac{\partial^2 u^{(s)}}{\partial X^2}+(1-2\nu)\frac{\partial^2 u^{(s)}}{\partial Y^2}+\frac{\partial^2 v^{(s)}}{\partial X\partial Y}=0, \tag{13a}$$

$$(1-2\nu)\frac{\partial^2 v^{(s)}}{\partial X^2}+2(1-\nu)\frac{\partial^2 v^{(s)}}{\partial Y^2}+\frac{\partial^2 u^{(s)}}{\partial X\partial Y}=0, \tag{13b}$$

which hold for $-\hat{L}\leq X\leq\hat{L}, -\infty<Y<-\hat{h}$. It should be observed that the notation

$$\hat{\alpha}=a\alpha, \qquad \hat{h}=h/a, \qquad \hat{L}=L/a$$

has been used above and that the shear modulus in the coating is now defined as

$$\mu(Y)=\mu_0 e^{\hat{\alpha}Y}.$$

A further transformation of the horizontal variable at this point is preferable so that the solid is mapped to the region $0\leq\zeta\leq\hat{L}, -\infty<Y\leq 0$. The requisite mapping here is

$$\zeta=\frac{1}{2}(X+\hat{L}) \tag{14}$$

and as a consequence

$$\frac{\partial}{\partial X}=\frac{\partial}{\partial\zeta}\frac{\mathrm{d}\zeta}{\mathrm{d}X}=\frac{1}{2}\frac{\partial}{\partial\zeta}. \tag{15}$$

The PDE's to be solved in this problem now become

$$\frac{1}{2}(1-\nu)\frac{\partial^2 u}{\partial\zeta^2}+\frac{1}{2}\frac{\partial^2 v}{\partial\zeta\partial Y}+(1-2\nu)\frac{\partial^2 u}{\partial Y^2}+\hat{\alpha}(1-2\nu)\frac{\partial u}{\partial Y}+\frac{1}{2}\hat{\alpha}(1-2\nu)\frac{\partial v}{\partial\zeta}=0, \tag{16a}$$

$$\frac{1}{2}\frac{\partial^2 u}{\partial\zeta\partial Y}+\frac{1}{4}(1-2\nu)\frac{\partial^2 v}{\partial\zeta^2}+\hat{\alpha}\nu\frac{\partial u}{\partial\zeta}+2\hat{\alpha}(1-\nu)\frac{\partial v}{\partial Y}+2(1-\nu)\frac{\partial^2 v}{\partial Y^2}=0 \tag{16b}$$

which must hold in the region $(0 \leq \zeta \leq \hat{L}, -\hat{h} \leq Y \leq 0)$ and

$$\frac{1}{2}(1-\nu)\frac{\partial^2 u}{\partial \zeta^2} + \frac{1}{2}\frac{\partial^2 v}{\partial \zeta \partial Y} + (1-2\nu)\frac{\partial^2 u}{\partial Y^2} = 0, \tag{17a}$$

$$\frac{1}{4}(1-2\nu)\frac{\partial^2 v}{\partial \zeta^2} + \frac{1}{2}\frac{\partial^2 u}{\partial \zeta \partial Y} + 2(1-\nu)\frac{\partial^2 v}{\partial Y^2} = 0, \tag{17b}$$

which must hold in $(0 \leq \zeta \leq \hat{L}, -\infty < y < -\hat{h})$. Under the transformation, the relevant boundary conditions can be written in terms of the displacements as

$$(1-\nu)\frac{\partial v}{\partial Y} + \frac{1}{2}\nu\frac{\partial u}{\partial \zeta} - \frac{a(1-2\nu)}{2\mu_0}P(\zeta) = 0, \qquad (Y=0), \tag{18a}$$

$$\frac{\partial u}{\partial Y} + \frac{1}{2}\frac{\partial v}{\partial \zeta} = 0, \qquad (Y=0), \tag{18b}$$

$$\frac{1}{2}(1-\nu)\frac{\partial u}{\partial \zeta} + \nu\frac{\partial v}{\partial Y} = v = 0, \qquad (\zeta=0), \tag{18c}$$

$$\frac{1}{2}(1-\nu)\frac{\partial u}{\partial \zeta} + \nu\frac{\partial v}{\partial Y} = v = 0, \qquad (\zeta=\hat{L}), \tag{18d}$$

$$\tag{18e}$$

whilst the relevant matching conditions yield

$$\frac{1}{2}\nu\frac{\partial u^{(c)}}{\partial \zeta} + (1-\nu)\frac{\partial v^{(c)}}{\partial Y} - \left(\frac{1}{2}\nu\frac{\partial u^{(s)}}{\partial \zeta} + (1-\nu)\frac{\partial v^{(s)}}{\partial Y}\right) = 0, \qquad (Y=-\hat{h}), \tag{19a}$$

$$\frac{\partial u^{(c)}}{\partial Y} + \frac{1}{2}\frac{\partial v^{(c)}}{\partial \zeta} - \left(\frac{\partial u^{(s)}}{\partial Y} + \frac{1}{2}\frac{\partial v^{(s)}}{\partial \zeta}\right) = 0, \qquad (Y=-\hat{h}), \tag{19b}$$

$$u^{(c)} - u^{(s)} = 0, \qquad (Y=-\hat{h}), \tag{19c}$$

$$v^{(c)} - v^{(s)} = 0, \qquad (Y=-\hat{h}). \tag{19d}$$

The problem is fully specified by imposing the radiation conditions $u, v \to 0$ as $Y \to -\infty$.

3. Method of solution

We look for simple separable solutions of the form

$$u(\zeta, Y) = A(Y)\cos(l\zeta) + B(Y)\sin(l\zeta), \tag{20a}$$

$$v(\zeta, Y) = C(Y)\cos(k\zeta) + D(Y)\sin(k\zeta), \tag{20b}$$

for $l, k > 0$ which we insist must satisfy the boundary conditions at $\zeta = 0$ and $\zeta = \hat{L}$. It is easily seen that there are an infinite number of solutions of the form

$$v(\zeta, Y) = \hat{B}_n(Y)\sin\left(\frac{n\pi\zeta}{\hat{L}}\right) \tag{21}$$

where $n \in \mathbb{N}$ which satisfy $v(0, Y) = v(\hat{L}, Y) = 0$. It is now seen that the other boundary conditions are satisfied if

$$\frac{\partial u}{\partial \zeta}(0, Y) = \frac{\partial u}{\partial \zeta}(\hat{L}, Y) = 0,$$

thus we see that taking

$$u(\zeta, Y) = \hat{A}_n(Y)\cos\left(\frac{n\pi\zeta}{\hat{L}}\right) + g_n(Y). \tag{22}$$

where $n \in \mathbb{N}$ ensures that the remaining conditions are satisfied. We note that as the boundary conditions on $\zeta = 0, \hat{L}$ are the same in the coating and the substrate, we may form the solution of the displacements in each region as

$$u(\zeta, Y) = \sum_{n=1}^{\infty} \hat{A}_n(Y)\cos(\beta_n\zeta) + g(\zeta), \tag{23a}$$

$$v(\zeta, Y) = \sum_{n=1}^{\infty} \hat{B}_n(Y)\sin(\beta_n\zeta). \tag{23b}$$

Note that the shorthand notation

$$\beta_n = \frac{n\pi}{\hat{L}}$$

has been used above for convenience.

It is now left to determine the Y-dependence of the displacements in both regions.

3.1. The coating

Substituting (23a) and (23b) into (16a) and (16b) yields the 2nd order ordinary differential equation (ODE)

$$g^{''} + \hat{\alpha} g^{'} = 0, \tag{24}$$

which admits the solution

$$g(y) = A_0^{(1)} + A_0^{(2)} e^{-\hat{\alpha} Y} \tag{25}$$

and the 2nd order ODE system

$$\begin{pmatrix} 1-2\nu & 0 \\ 0 & 2(1-\nu) \end{pmatrix} \begin{pmatrix} \hat{A}_n^{''} \\ \hat{B}_n^{''} \end{pmatrix} + \begin{pmatrix} \hat{\alpha}(1-2\nu) & \frac{1}{2}\beta_n \\ -\frac{1}{2}\beta_n & 2\hat{\alpha}(1-\nu) \end{pmatrix} \begin{pmatrix} \hat{A}_n^{'} \\ \hat{B}_n^{'} \end{pmatrix} + \begin{pmatrix} -\frac{1}{2}(1-\nu)\beta_n^2 & \frac{1}{2}\hat{\alpha}(1-2\nu)\beta_n \\ -\hat{\alpha}\nu\beta_n & -\frac{1}{4}(1-2\nu)\beta_n^2 \end{pmatrix} \begin{pmatrix} \hat{A}_n \\ \hat{B}_n \end{pmatrix} = 0, \tag{26}$$

where $'$ denotes differentiation with respect to Y and $n \in \mathbb{N}$. Assuming that n is fixed, letting $F = (\hat{A}_n, \ \hat{B}_n)^T$, $G = (\hat{A}_n^{'}, \ \hat{B}_n^{'})^T$ and $Z = (F, \ G)^T$ allows us to write (26) as the first order system

$$Z^{'} = MZ \tag{27}$$

where M is the 4×4 block matrix

$$M=\begin{pmatrix} 0 & I \\ -T & -S \end{pmatrix}.$$

Note that 0 and I denote the 2×2 zero matrix and identity matrix respectively, whilst the other matrices are defined as

$$S=\begin{pmatrix} \hat{\alpha} & \frac{\beta_n}{2(1-2\nu)} \\ -\frac{\beta_n}{4(1-\nu)} & \hat{\alpha} \end{pmatrix}$$

$$T=\begin{pmatrix} -\frac{(1-\nu)\beta_n^2}{2(1-2\nu)} & \frac{1}{2}\hat{\alpha}\beta_n \\ -\frac{\hat{\alpha}\nu\beta_n}{2(1-\nu)} & -\frac{(1-2\nu)\beta_n^2}{8(1-\nu)}. \end{pmatrix}.$$

This system may be solved by seeking solutions of the form

$$Z=C\mathsf{e}^{\lambda \mathsf{Y}}, \tag{28}$$

which when substituted into (27) gives

$$(M-\lambda I)C\mathsf{e}^{\lambda \mathsf{Y}}=0. \tag{29}$$

It is immediately seen that $\mathrm{Det}(M-\lambda I)=0$ in order to obtain non-trivial solutions to this problem and thus we seek the eigenvalues λ of M. Some straightforward calculations show that λ satisfies the quartic equation

$$\lambda^4+2\hat{\alpha}\lambda^3+\left(\hat{\alpha}^2-\frac{1}{2}\beta_n^2\right)\lambda^2-\frac{1}{2}\hat{\alpha}\beta_n^2\lambda+\frac{\beta_n^2}{16}(\beta_n^2+4\hat{\alpha}^2\rho)=0, \tag{30}$$

where $\rho = \nu/(1-\nu)$. The roots of this equation are found to be

$$\lambda_{1,n} = \sqrt{\frac{1}{4}(\hat{\alpha}^2+\beta_n^2)+\frac{i}{2}\hat{\alpha}\beta_n\sqrt{\rho}} - \frac{1}{2}\hat{\alpha}, \tag{31a}$$

$$\lambda_{2,n} = -\sqrt{\frac{1}{4}(\hat{\alpha}^2+\beta_n^2)+\frac{i}{2}\hat{\alpha}\beta_n\sqrt{\rho}} - \frac{1}{2}\hat{\alpha}, \tag{31b}$$

$$\lambda_{3,n} = \sqrt{\frac{1}{4}(\hat{\alpha}^2+\beta_n^2)-\frac{i}{2}\hat{\alpha}\beta_n\sqrt{\rho}} - \frac{1}{2}\hat{\alpha}, \tag{31c}$$

$$\lambda_{4,n} = -\sqrt{\frac{1}{4}(\hat{\alpha}^2+\beta_n^2)-\frac{i}{2}\hat{\alpha}\beta_n\sqrt{\rho}} - \frac{1}{2}\hat{\alpha}, \tag{31d}$$

so we see that $\lambda_{3,n} = \bar{\lambda}_{1,n}$, $\lambda_{4,n} = \bar{\lambda}_{2,n}$. We can now write down explicitly the solutions of $\hat{A}_n(Y)$ and $\hat{B}_n(Y)$ as

$$\hat{A}_n(Y) = A_n^{(1)}e^{\lambda_{1,n}Y} + A_n^{(2)}e^{\lambda_{2,n}Y} + A_n^{(3)}e^{\lambda_{3,n}Y} + A_n^{(4)}e^{\lambda_{4,n}Y}, \tag{32}$$

$$\hat{B}_n(Y) = B_n^{(1)}e^{\lambda_{1,n}Y} + B_n^{(2)}e^{\lambda_{2,n}Y} + B_n^{(3)}e^{\lambda_{3,n}Y} + B_n^{(4)}e^{\lambda_{4,n}Y}, \tag{33}$$

which are valid in the region $(-\hat{h} \le Y \le 0)$. Combining all individual solutions allows us to form the general solutions

$$u^{(c)}(\zeta,Y) = A_0^{(1)} + A_0^{(2)}e^{-\hat{\alpha}Y} + \sum_{n=1}^{\infty}(A_n^{(1)}e^{\lambda_{1,n}Y} + A_n^{(2)}e^{\lambda_{2,n}Y} + A_n^{(3)}e^{\lambda_{3,n}Y} + A_n^{(4)}e^{\lambda_{4,n}Y})\cos(\beta_n\zeta), \tag{34a}$$

$$v^{(c)}(\zeta,Y) = \sum_{n=1}^{\infty}(B_n^{(1)}e^{\lambda_{1,n}Y} + B_n^{(2)}e^{\lambda_{2,n}Y} + B_n^{(3)}e^{\lambda_{3,n}Y} + B_n^{(4)}e^{\lambda_{4,n}Y})\sin(\beta\zeta), \tag{34b}$$

valid in the region $(0 \le \zeta \le \hat{L}, -\hat{h} \le Y \le 0)$. Substituting (34a) and (34b) into (16a) and (16b) reveals that the constants $A_j^{(n)}$ and $B_j^{(n)}$ are dependent and related via

$$B_j^{(n)} = -\gamma_{j,n}A_j^{(n)} \tag{35}$$

where

$$\gamma_{j,n} = \frac{2\left((1-2\nu)\lambda_{j,n}^2 + \hat{\alpha}(1-2\nu)\lambda_{j,n} - \frac{1}{2}(1-\nu)\beta_n^2\right)}{\beta_n\left(\lambda_{j,n} + \hat{\alpha}(1-2\nu)\right)}, \tag{36}$$

$j = 1,...,4, n \in \mathbb{N}$.

3.2. The substrate

Substituting (23a), (23b) into (17a) and (17b) yields the 2nd order differential equation

$$(1-2\nu)g_2'' = 0 \tag{37}$$

and the coupled system of 2nd order differential equations

$$\begin{pmatrix} 1-2\nu & 0 \\ 0 & 2(1-\nu) \end{pmatrix} \begin{pmatrix} \hat{A}_n'' \\ \hat{B}_n'' \end{pmatrix} + \begin{pmatrix} 0 & \frac{1}{2}\beta_n \\ -\frac{1}{2}\beta_n & \end{pmatrix} \begin{pmatrix} \hat{A}_n' \\ \hat{B}_n' \end{pmatrix} - \begin{pmatrix} \frac{1}{2}(1-\nu)\beta_n^2 & 0 \\ 0 & \frac{1}{4}(1-2\nu)\beta_n^2 \end{pmatrix} \begin{pmatrix} \hat{A}_n \\ \hat{B}_n \end{pmatrix} = 0, \tag{38}$$

where $n \in \mathbb{N}$. Following the solution method outlined in the previous section, we find that in the region $(-\infty < Y < -\hat{h})$

$$u^{(s)}(\zeta, Y) = C_0^{(1)} + C_0^{(2)} Y + \sum_{n=1}^{\infty} \left\{ \left(C_n^{(1)} + C_n^{(2)} Y \right) e^{\frac{1}{2}\beta_n Y} + \left(C_n^{(3)} + C_n^{(4)} Y \right) e^{-\frac{1}{2}\beta_n Y} \right\} \cos(\beta_n \zeta), \tag{39a}$$

$$v^{(s)}(\zeta, Y) = \sum_{n=1}^{\infty} \left\{ \left(D_n^{(1)} + D_n^{(2)} Y \right) e^{\frac{1}{2}\beta_n Y} + \left(D_n^{(3)} + D_n^{(4)} Y \right) e^{-\frac{1}{2}\beta_n Y} \right\} \sin(\beta_n \zeta). \tag{39b}$$

It should immediately be noticed that in order to obtain a bounded solution to this problem as $Y \to -\infty$, we must set $C_0^{(2)} = C_n^{(3)} = C_n^{(4)} = D_n^{(3)} = D_n^{(4)} = 0 \; \forall n \in \mathbb{N}$. Additionally, we can only satisfy the condition $u \to 0$ as $Y \to -\infty$ if $C_0^{(1)} = 0$. The revised general solution of the displacements in

the substrate are now

$$u^{(s)}(\zeta,Y)=\sum_{n=1}^{\infty}\left(C_n^{(1)}+C_n^{(2)}Y\right)e^{\frac{1}{2}\beta_n Y}\cos(\beta_n\zeta), \tag{40a}$$

$$v^{(s)}(\zeta,Y)=\sum_{n=1}^{\infty}\left(D_n^{(1)}+D_n^{(2)}Y\right)e^{\frac{1}{2}\beta_n Y}\sin(\beta_n\zeta). \tag{40b}$$

Note that the constants in this solution are related via

$$D_n^{(1)}=C_n^{(1)}-\delta_n C_n^{(2)}, \tag{41a}$$

$$D_n^{(2)}=C_n^{(2)}, \tag{41b}$$

where

$$\delta_n=\frac{2(3-4\nu)}{\beta_n}. \tag{42}$$

We exploit the constant relationships in both the coating and the substrate in the next section.

3.3. Determination of the final solution

It is now left to determine the remaining constants in the problem. Applying the matching conditions given in (19) and using (34a), (34b), (40a) and (40b) gives the relations

$$\begin{pmatrix} C_n^{(1)} \\ C_n^{(2)} \end{pmatrix}=\frac{e^{\frac{1}{2}\beta_n\hat{h}}}{\delta_n}\left\{Z_{1,n}\mathscr{K}_{1,n}\begin{pmatrix} A_n^{(1)} \\ A_n^{(3)} \end{pmatrix}+Z_{2,n}\mathscr{K}_{2,n}\begin{pmatrix} A_n^{(2)} \\ A_n^{(4)} \end{pmatrix}\right\}, \tag{43}$$

$$\begin{pmatrix} A_n^{(2)} \\ A_n^{(4)} \end{pmatrix}=-\mathscr{K}_{2,n}^{-1}\left(N_{2,n}+\frac{1}{\delta_n}M_{2,n}\right)^{-1}\left(N_{1,n}+\frac{1}{\delta_n}M_{1,n}\right)\mathscr{K}_{1,n}\begin{pmatrix} A_n^{(1)} \\ A_n^{(3)} \end{pmatrix}, \tag{44}$$

where

$$\mathscr{K}_{j,n} = \begin{pmatrix} e^{-\lambda_{j,n}\hat{h}} & 0 \\ 0 & e^{-\lambda_{j+2,n}\hat{h}} \end{pmatrix}, \tag{45a}$$

$$Z_{j,n} = \begin{pmatrix} \delta_n + \hat{h}\tau_{j,n} & \delta_n + \hat{h}\tau_{j+2,n} \\ \tau_{j,n} & \tau_{j+2,n} \end{pmatrix}, \tag{45b}$$

$$M_{j,n} = \begin{pmatrix} \frac{1}{2}(1-2\nu)\left(4(1-\nu)\tau_{j,n} - \beta_n\delta_n\right) & \frac{1}{2}(1-2\nu)\left(4(1-\nu)\tau_{j+2,n} - \beta_n\delta_n\right) \\ 2(1-2\nu)\tau_{j,n} - \beta_n\delta_n & 2(1-2\nu)\tau_{j+2,n} - \beta_n\delta_n \end{pmatrix}, \tag{45c}$$

$$N_{j,n} = \begin{pmatrix} -\left(\frac{1}{2}\nu\beta_n + (1-\nu)\lambda_{j,n}\gamma_{j,n}\right) & -\left(\frac{1}{2}\nu\beta_n + (1-\nu)\lambda_{j+2,n}\gamma_{j+2,n}\right) \\ \lambda_{j,n} - \frac{1}{2}\beta_n\gamma_{j,n} & \lambda_{j+2,n} - \frac{1}{2}\beta_n\gamma_{j+2,n} \end{pmatrix}, \tag{45d}$$

for $j = 1, 2$ and

$$\tau_{j,n} = 1 + \gamma_{j,n} \tag{46}$$

for $j = 1, 2, 3, 4$. It is now only left to apply the surface conditions at $Y = 0$. Substituting (34a), (34b), (40a) and (40b) into the boundary conditions applied on $Y = 0$ in equation (18) gives

$$N_{1,n}\begin{pmatrix} A_n^{(1)} \\ A_n^{(3)} \end{pmatrix} + N_{2,n}\begin{pmatrix} A_n^{(2)} \\ A_n^{(4)} \end{pmatrix} = \begin{pmatrix} \frac{a(1-2\nu)}{2\mu_0}P_n \\ 0 \end{pmatrix}. \tag{47}$$

The coefficients P_n, $n \in \mathbb{N}$ define the coefficients in the Fourier sine series of $P(\zeta)$ and are defined as

$$P_n = -\frac{2}{\hat{L}}\int_{\frac{1}{2}(\hat{L}-1)}^{\frac{1}{2}(\hat{L}+1)} p(\zeta)\sin(\beta_n\zeta)\mathrm{d}\zeta. \tag{48}$$

Combining (44) and (47) reveals that

$$\begin{pmatrix} A_n^{(1)} \\ A_n^{(3)} \end{pmatrix} = W_n^{-1}\begin{pmatrix} \frac{a(1-2\nu)}{2\mu_0}P_n \\ 0 \end{pmatrix}, \tag{49}$$

with

$$W_n = N_{1,n} - N_{2,n}(T_{2,n}\mathscr{K}_{2,n})^{-1}T_{1,n}\mathscr{K}_{1,n}, \tag{50}$$

$$T_{j,n} = \left(N_{j,n} + \frac{1}{\delta_n}M_{j,n}\right) \tag{51}$$

for $j = 1,2$. Further use of (43) and (44) yields

$$\begin{pmatrix} A_n^{(2)} \\ A_n^{(4)} \end{pmatrix} = -(T_{2,n}\mathscr{K}_{2,n})^{-1}T_{1,n}\mathscr{K}_{1,n}W_n^{-1}\begin{pmatrix} \frac{a(1-2\nu)}{2\mu_0}P_n \\ 0 \end{pmatrix}, \tag{52}$$

$$\begin{pmatrix} C_n^{(1)} \\ C_n^{(2)} \end{pmatrix} = \frac{e^{\frac{1}{2}\beta_n\hat{h}}}{\delta_n}\left(Z_{1,n} - Z_{2,n}T_{2,n}^{-1}T_{1,n}\right)K_{1,n}W_n^{-1}\begin{pmatrix} \frac{a(1-2\nu)}{2\mu_0}P_n \\ 0 \end{pmatrix}. \tag{53}$$

As we have now determined all of the constants appearing in this problem, we may now construct the final solution of the displacements in the transformed problem as

$$u(\zeta,Y) = \sum_{n=1}^{\infty}\xi_n^T(Y)\Omega_n\begin{pmatrix} \frac{a(1-2\nu)}{2\mu_0}P_n \\ 0 \end{pmatrix}\cos(\beta_n\zeta), \tag{54a}$$

$$v(\zeta,Y) = -\sum_{n=1}^{\infty}\xi_n^T(Y)\Gamma_n\Omega_n\begin{pmatrix} \frac{a(1-2\nu)}{2\mu_0}P_n \\ 0 \end{pmatrix}\sin(\beta_n\zeta) \tag{54b}$$

which holds in the region $0 \leq \zeta \leq \hat{L}, -\hat{h} \leq Y \leq 0$ and

$$u(\zeta,Y) = \sum_{n=1}^{\infty}\varphi^T(Y)\Theta_n\begin{pmatrix} \frac{a(1-2\nu}{2\mu_0}P_n \\ 0 \end{pmatrix}\frac{e^{\frac{1}{2}\beta_n(Y+\hat{h})}}{\delta_n}\cos(\beta_n\zeta), \tag{55a}$$

$$v(\zeta,Y) = \sum_{n=1}^{\infty}\varphi^T(Y)J_n\Theta_n\begin{pmatrix} \frac{a(1-2\nu)}{2\mu_0}P_n \\ 0 \end{pmatrix}\frac{e^{\frac{1}{2}\beta_n(Y+\hat{h})}}{\delta_n}\sin(\beta_n\zeta), \tag{55b}$$

which is valid for $0 \leq \zeta \leq \hat{L}, -\infty < Y < -\hat{h}$. The quantities appearing in the above equations are

$$\varphi(Y) = (1, \ \ Y)^T, \tag{56a}$$

$$\xi_n(y) = \left(e^{\lambda_{1,n}y}, \ \ e^{\lambda_{3,n}y}, \ \ e^{\lambda_{2,n}y}, \ \ e^{\lambda_{4,n}y}\right)^T, \tag{56b}$$

$$\Gamma_n = \mathrm{diag}(\gamma_{1,n}, \gamma_{3,n}, \gamma_{2,n}, \gamma_{4,n}), \tag{56c}$$

$$\Omega_n = \begin{pmatrix} W_n^{-1} \\ -(T_{2,n}\mathscr{K}_{2,n})^{-1}T_{1,n}\mathscr{K}_{1,n}W_n^{-1} \end{pmatrix}, \tag{56d}$$

$$\Theta_n = \left(Z_{1,n} - Z_{2,n}T_{2,n}^{-1}T_{1,n}\right)K_{1,n}W_n^{-1}, \tag{56e}$$

$$J_n = \begin{pmatrix} 1 & -\delta_n \\ 0 & 1 \end{pmatrix}, \tag{56f}$$

for $n \in \mathbb{N}$.

Re-writing (54a), (54b), (55a) and (55b) in terms of the X-coordinate gives the solution of the original problem as

$$u(X,Y) = \sum_{n=1}^{\infty} \xi_n^T(Y)\Omega_n \begin{pmatrix} \frac{a(1-2\nu)}{2\mu_0}P_n \\ 0 \end{pmatrix} \cos\left(\frac{1}{2}\beta_n(X+\hat{L})\right), \tag{57a}$$

$$v(X,Y) = -\sum_{n=1}^{\infty} \xi_n^T(Y)\Gamma_n\Omega_n \begin{pmatrix} \frac{a(1-2\nu)}{2\mu_0}P_n \\ 0 \end{pmatrix} \sin\left(\frac{1}{2}\beta_n(X+\hat{L})\right) \tag{57b}$$

in $(-\hat{h} \leq Y \leq 0, -\hat{L} \leq X \leq \hat{L})$ and

$$u(X,Y) = \sum_{n=1}^{\infty} \varphi^T(Y)\Theta_n \begin{pmatrix} \frac{a(1-2\nu)}{2\mu_0} P_n \\ 0 \end{pmatrix} \frac{e^{\frac{1}{2}\beta_n(Y+\hat{h})}}{\delta_n} \cos\left(\frac{1}{2}\beta_n(X+\hat{L})\right), \tag{58a}$$

$$v(X,Y) = \sum_{n=1}^{\infty} \varphi^T(Y)J_n\Theta_n \begin{pmatrix} \frac{a(1-2\nu)}{2\mu_0} P_n \\ 0 \end{pmatrix} \frac{e^{\frac{1}{2}\beta_n(Y+\hat{h})}}{\delta_n} \sin\left(\frac{1}{2}\beta_n(X+\hat{L})\right), \tag{58b}$$

in $(-\infty < Y < -\hat{h}, -\hat{L} \leq X \leq \hat{L})$.

Using (54a), (54b), (55a) and (55b), we can calculate the partial derivatives necessary to use in (9a)-(9c) and thus determine the stresses within the solid. In particular, the principal stress defined as

$$\tau_1 = \frac{1}{2}\sqrt{(\sigma_{xx} - \sigma_{yy})^2 + 4\sigma_{xy}^2} \tag{59}$$

will be investigated extensively in Section 5.

3.4. Limiting cases

The solutions for the displacements given above are valid for all possible values of $\hat{h}$. It is noticeable however that the expressions for the constants in both the coating and substrate are somewhat cumbersome and it is difficult to determine to what extent $\hat{h}$ affects the stresses and displacements within the problem. This issue can be simplified if the coating is considered to be very thick ($\hat{h} \to \infty$).

We initially note that in the coating, only the matrices $\mathscr{K}_{1,n}$ and $\mathscr{K}_{2,n}$ depend on $\hat{h}$. Denoting

$R_n = T_{2,n}^{-1} T_{1,n}$ where $n \in \mathbb{N}$, we see that

$$\mathscr{K}_{2.n}^{-1} R_n \mathscr{K}_{1,n} = \begin{pmatrix} R_n^{11} e^{(\lambda_{2,n}-\lambda_{1,n})\hat{h}} & R_n^{12} e^{(\lambda_{2,n}-\lambda_{3,n})\hat{h}} \\ R_n^{21} e^{(\lambda_{4,n}-\lambda_{1,n})\hat{h}} & R_n^{22} e^{(\lambda_{4,n}-\lambda_{3,n})\hat{h}} \end{pmatrix} \to 0, \qquad \hat{h} \to 0,$$

where the superscript notation indicates the position of each entry in matrix R_n. We can use this information to determine that $W_n \to N_{1,n}$ as $\hat{h} \to \infty$ and further that

$$\begin{pmatrix} A_n^{(1)}, \\ A_n^{(3)} \end{pmatrix} \to N_{1,n}^{-1} \begin{pmatrix} \frac{a(1-2\nu)}{2\mu_0} P_n \\ 0 \end{pmatrix}$$

$$\begin{pmatrix} A_n^{(2)}, \\ A_n^{(4)} \end{pmatrix} \to 0$$

as $\hat{h} \to \infty$. The resulting solutions in the coating are

$$u(X,Y) = \sum_{n=1}^{\infty} (e^{\lambda_{1,n}Y}, e^{\lambda_{3,n}Y}) N_{1,n}^{-1} \begin{pmatrix} \frac{a(1-2\nu)}{2\mu_0} P_n \\ 0 \end{pmatrix} \cos\left(\frac{1}{2}\beta_n(X+\hat{L})\right), \tag{60}$$

$$v(X,Y) = -\sum_{n=1}^{\infty} (e^{\lambda_{1,n}Y}, e^{\lambda_{3,n}Y}) \begin{pmatrix} \gamma_{1.n} & 0 \\ 0 & \gamma_{3,n} \end{pmatrix} N_{1,n}^{-1} \begin{pmatrix} \frac{a(1-2\nu)}{2\mu_0} P_n \\ 0 \end{pmatrix} \sin\left(\frac{1}{2}\beta_n(X+\hat{L})\right). \tag{61}$$

It can be verified that this solution corresponds to the contact problem of a pressure force being applied normally to the surface of a semi-infinite graded elastic solid and is equivalent to the solution presented by Chidlow et al., 2010

A further simplification of this solution is possible if $\hat{\alpha} \ll 1$. In this situation, we can seek asymptotic approximations to the roots $\lambda_{j.n}$ in the form

$$\lambda_{j,n} = \sum_{m=0}^{\infty} \lambda_m^{j,n} \hat{\alpha}^m, \tag{62}$$

where $\lambda_m^{j,n}$ are (possibly complex) constant coefficients. Substituting (62) into (30) yields the expressions

$$\lambda_{1,n} = \frac{1}{2}\left(\beta_n - (1 - i\sqrt{\rho})\hat{\alpha}\right) + \mathrm{O}(\hat{\alpha}^2), \tag{63a}$$

$$\lambda_{3,n} = \frac{1}{2}\left(\beta_n - (1 + i\sqrt{\rho})\hat{\alpha}\right) + \mathrm{O}(\hat{\alpha}^2), \tag{63b}$$

which can be further used to give

$$\gamma_{1,n} = -1 - \frac{\hat{\alpha}}{\beta_n}\left(1 + i\sqrt{\rho}(3-4\nu)\right) + \mathrm{O}(\hat{\alpha}^2),$$

$$\gamma_{3,n} = -1 - \frac{\hat{\alpha}}{\beta_n}\left(1 - i\sqrt{\rho}(3-4\nu)\right) + \mathrm{O}(\hat{\alpha}^2),$$

and thus

$$N_{1,n} = \begin{pmatrix} \frac{1}{2}(1-2\nu)(\beta_n + 2i(1-\nu)\sqrt{\rho}\hat{\alpha}) & \frac{1}{2}(1-2\nu)(\beta_n - 2i(1-\nu)\sqrt{\rho}\hat{\alpha}) \\ \beta_n + i(1-2\nu)\sqrt{\rho}\hat{\alpha} & \beta_n - i(1-2\nu)\sqrt{\rho}\hat{\alpha} \end{pmatrix} + \mathrm{O}(\hat{\alpha}^2).$$

Substituting these results into (60) and (61) yields the asymptotic solutions

$$\begin{aligned} u(X,Y) = -\sum_{n=1}^{\infty} \frac{aP_n}{\mu_0\sqrt{\rho}\beta_n\hat{\alpha}} e^{\frac{1}{2}(\beta_n - \hat{\alpha})Y} \Bigg(& \beta_n \sin\left(\frac{1}{2}\sqrt{\rho}\hat{\alpha}Y\right) \\ & + (1-2\nu)\sqrt{\rho}\hat{\alpha}\cos\left(\frac{1}{2}\sqrt{\rho}\hat{\alpha}Y\right) + \mathrm{O}(\hat{\alpha}^2)\Bigg)\cos\left(\frac{1}{2}\beta_n(X+\hat{L})\right), \\ v(X,Y) = -\sum_{n=1}^{\infty} \frac{aP_n}{\mu_0\sqrt{\rho}\beta_n\hat{\alpha}} e^{\frac{1}{2}(\beta_n - \hat{\alpha})y} \Bigg(& (\beta_n + \hat{\alpha})\sin\left(\frac{1}{2}\sqrt{\rho}\hat{\alpha}Y\right) \\ & - 2(1-\nu)\sqrt{\rho}\hat{\alpha}\cos\left(\frac{1}{2}\sqrt{\rho}\hat{\alpha}Y\right) + \mathrm{O}(\hat{\alpha}^2)\Bigg)\sin\left(\frac{1}{2}\beta_n(X+\hat{L})\right). \end{aligned}$$

Provided that $Y \neq \mathrm{O}(1/\hat{\alpha})$ which is certainly true close to the solid surface, we can replace the functions involving $\hat{\alpha}$ by their taylor series and thus we find that

$$\begin{aligned} u(X,Y) &= -\sum_{n=1}^{\infty} \frac{aP_n}{\beta_n\mu_0} e^{\frac{1}{2}\beta_n Y}\left((1-2\nu) + \frac{1}{2}\beta_n Y\right)\cos\left(\frac{1}{2}\beta_n(X+\hat{L})\right) + \mathrm{O}(\hat{\alpha}), \\ v(X,Y) &= \sum_{n=1}^{\infty} \frac{aP_n}{\mu_0} e^{\frac{1}{2}\beta_n Y}\left(2(1-\nu) - \frac{1}{2}\beta_n Y\right)\sin\left(\frac{1}{2}\beta_n(X+\hat{L})\right) + \mathrm{O}(\hat{\alpha}). \end{aligned}$$

These solutions correspond to the contact problem involving a homogeneously stiff media with small correction terms of $0(\hat{\alpha})$ detailing the effects of the inhomogeneity of the solid.

4. Implementation - Analytical and Discrete Pressure functions

The solutions presented in the previous section for the dimensionless displacements $u(X,Y)$, $v(X,Y)$ and consequently the stresses present in the solid resulting from the applied surface pressure involve infinite summations. However, in practice, we are restricted to summing only finitely many Fourier modes. As a result, we re-define the solution of the displacements as

$$u(X,Y) = \sum_{n=1}^{N} \xi_n^T(Y)\Omega_n \begin{pmatrix} \frac{a(1-2\nu)}{2\mu_0}P_n \\ 0 \end{pmatrix} \cos\left(\frac{1}{2}\beta_n(X+\hat{L})\right), \tag{64a}$$

$$v(X,Y) = -\sum_{n=1}^{N} \xi_n^T(Y)\Gamma_n\Omega_n \begin{pmatrix} \frac{a(1-2\nu)}{2\mu_0}P_n \\ 0 \end{pmatrix} \sin\left(\frac{1}{2}\beta_n(X+\hat{L})\right) \tag{64b}$$

in $(-\hat{h} \leq Y \leq 0, -\hat{L} \leq X \leq \hat{L})$ and

$$u(X,Y) = \sum_{n=1}^{N} \varphi^T(Y)\Theta_n \begin{pmatrix} \frac{a(1-2\nu)}{2\mu_0}P_n \\ 0 \end{pmatrix} \frac{e^{\frac{1}{2}\beta_n(Y+\hat{h})}}{\delta_n} \cos\left(\frac{1}{2}\beta_n(X+\hat{L})\right), \tag{65a}$$

$$v(X,Y) = \sum_{n=1}^{N} \varphi^T(Y)J_n\Theta_n \begin{pmatrix} \frac{a(1-2\nu)}{2\mu_0}P_n \\ 0 \end{pmatrix} \frac{e^{\frac{1}{2}\beta_n(Y+\hat{h})}}{\delta_n} \sin\left(\frac{1}{2}\beta_n(X+\hat{L})\right), \tag{65b}$$

in $(-\infty < Y < -\hat{h}, -\hat{L} \leq X \leq \hat{L})$. The number N is a positive integer which is determined at the start of the analysis by the user.

The solution detailed in this paper is valid for any pressure function $p(x)$ which obeys the criteria for having a Fourier series decomposition in $-a \leq x \leq a$. However, the principal advantage

of this method is that if the applied pressure is known exactly then the solution of the displacements given above is analytic. Typically though, the pressure applied to the surface of the solid will not be known exactly and will probably have been determined numerically. This could potentially mean that the given pressure is discrete and only known at finitely many points (which may or may not be equidistant).

In such a situation, the method given outlined in this paper may still be used to solve the contact problem provided that the pressure function is made continuous. A good way of doing this is to fit a polynomial spline to the discrete pressure data. Assuming that the pressure inputted into the problem is known at M points in the interval $[-a,a]$ where $x_1 = -a$, $x_M = a$ and $p(x_j) \approx p_j$ for $j = 1,...,M$, the simplest choice is to fit a linear spline (see Suli and Mayers, 2003, for example) so that

$$p(x) = \sum_{j=1}^{M} p_j \phi_j(x). \tag{66}$$

The functions $\phi_j(x)$ are chosen such that

$$\phi_j(x) = \begin{cases} 1, & x_i = x_j, \\ 0, & x_i \neq x_j \end{cases} \tag{67}$$

where $i, j = 1,..,M$. The Fourier coefficients can still be calculated from here as

$$\begin{aligned} P_n &= -\frac{1}{L}\int_{-a}^{a} p(x)\sin\left(\frac{n\pi}{2L}(x+L)\right)\mathrm{d}x, \\ &= -\frac{1}{L}\sum_{j=1}^{M} p_j \int_{-a}^{a} \phi_j(x)\sin\left(\frac{n\pi}{2L}(x+L)\right)\mathrm{d}x \end{aligned} \tag{68}$$

for $n = 1,...N$.

Figure (2) outlines the main steps required to compute the sub-surface stresses and displace-

ments using this method. This roadmap should help anyone aiming to implement this solution technique in a practical problem.

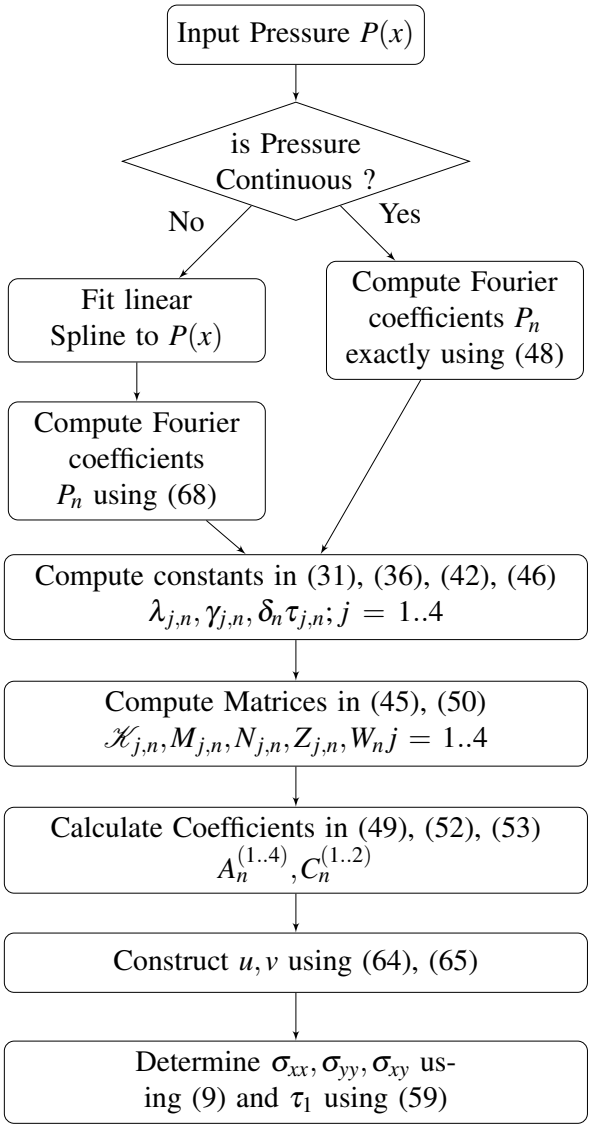

Figure 2: Flow chart of the Solution Method

5. Numerical results and discussions

We consider a pressure function which is very simple in form to produce results for the contact problem. The chosen pressure is defined as

$$p(x) = p_0 \sin\left(\frac{(x+a)\pi}{2a}\right) \tag{69}$$

which is symmetric about $x = 0$ and is continuous at $x = \pm a$. The corresponding dimensionless version of (69) can be easily verified as

$$p(X) = p_0 \sin\left(\frac{(X+1)\pi}{2}\right) \tag{70}$$

which is presented in figure (3). The principal advantage of the method outlined in this paper is that provided the pressure applied to the solid is analytic, the Fourier coefficients P_n, $n \in \mathbb{N}$ can be calculated exactly and thus the displacements u and v are given analytically. In this particular example,the Fourier coefficients can be readily calculated as

$$P_{2m-1} = \frac{4\hat{L}(-1)^m}{\pi\left((2m-1)^2 - \hat{L}^2\right)} \cos\left(\frac{(2m-1)\pi}{2\hat{L}}\right), \tag{71}$$

$$P_{2m} = 0, \tag{72}$$

for $m \geq 1$, so that the stresses and displacements inherent in this problem consist of only odd numbered Fourier modes.

Our aim in this example is to investigate the impact of different coatings on the sub-surface stress field resulting from the contact problem and thus the parameter values $\hat{\alpha}$ and $\hat{h}$ will be allowed to vary between problems. The value $\nu = 0.25$ will remain fixed throughout this example.

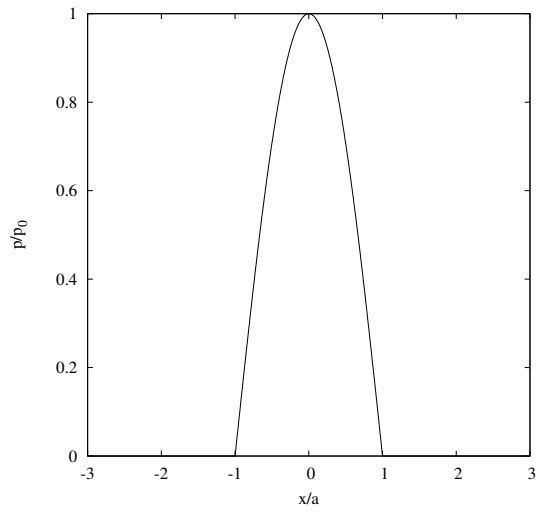

Figure 3: Applied pressure $p(x)$ over the dimensionless contact region $[-3,3]$

5.1. Choosing the optimal value for $\hat{L}$

The ability to choose a suitable length interval over which to solve the contact problem is vital to the success of this method. The underlying assumption in the derivation of this model is that the stresses within the solid resulting from the application of surface pressure decay very quickly away from the contact region and hence only a small piece of the solid is affected by the contact pressure. We have taken the dimensionless length of this piece of the solid to be $2\hat{L}$.

The greatest challenge in implementing the solution method described here is determining an appropriate value of $\hat{L}$. It should be observed that whilst the predicted solution is likely to become more accurate as $\hat{L}$ increases, the computational time will increase as well. Therefore, the optimal value of $\hat{L}$ is a compromise between accuracy and computational expense.

Figure (4) shows the maximum dimensionless principal stress $\max(\tau_1/p_0)$ plotted against $\hat{L}$ for three different coatings $\mu_1/\mu_0 = 0.25, 0.5, 2$ of three different thicknesses $\hat{h} = 0.2, 0.5, 1$. It may be seen that $\max(\tau_1/p_0)$ converges as $\hat{L}$ increases and in particular choosing $\hat{L} = 8$ leads to solutions

with error of less than 2%, whilst choosing $\hat{L} = 10$ gives solutions with an error of less than 1%. The choice $\hat{L} = 10$ will be used in all of the results that follow.

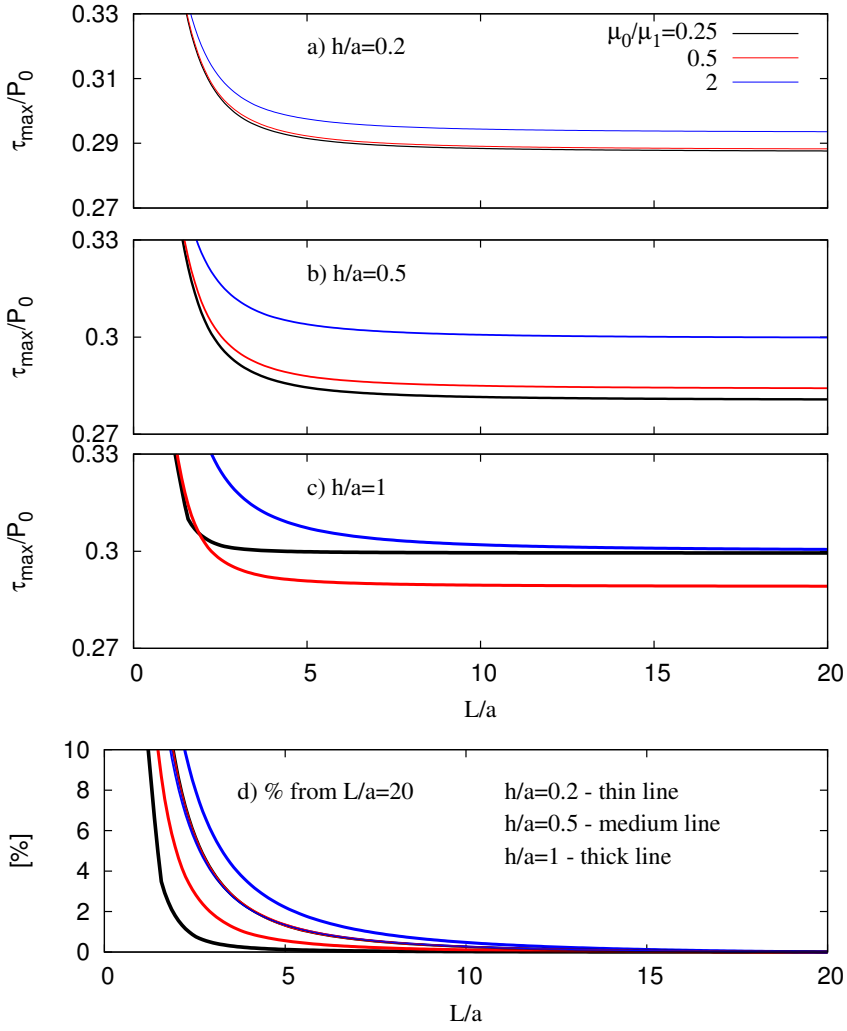

Figure 4: a)-c) are plots of $\max(\tau_1/p_0)$ against $\hat{L}$ for coatings with different shear modulus subject to thicknesses a) $\hat{h} = 0.2$ (thin coating), b) $\hat{h} = 0.5$ (medium coating) and c) $\hat{h} = 1$ (thick coating). d) shows the percentage error between the results produced using different values of $\hat{L}$ and the reference value $\hat{L} = 20$.

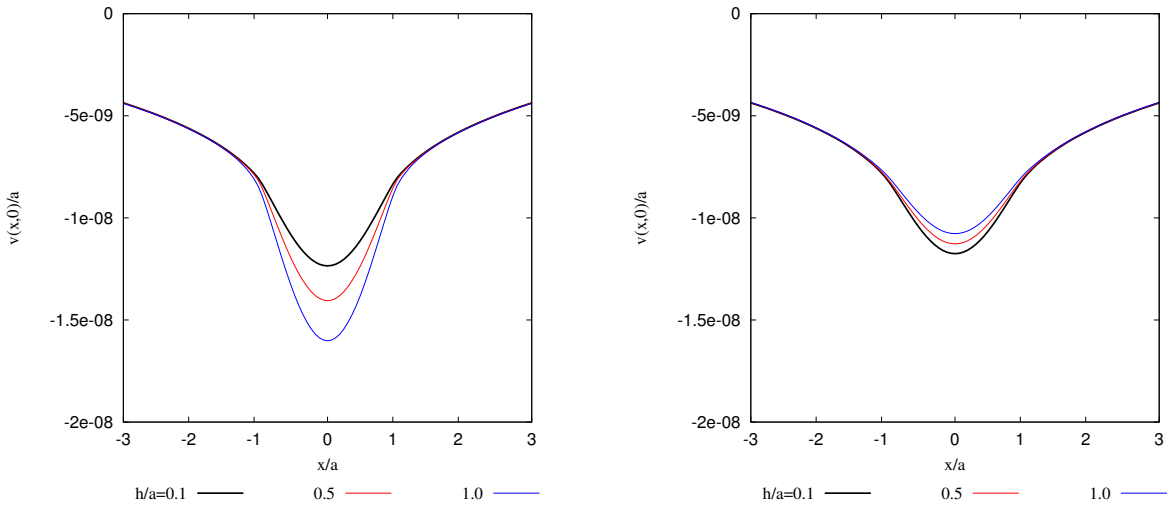

(a) $\mu_1/\mu_0 = 0.25$ (b) $\mu_1/\mu_0 = 2$

Figure 5: Surface deflection $v(x,0)$ over the dimensionless contact region $[-3,3]$

Figure (5a) shows the surface deflection $v(X,0)$ for the soft coating $\mu_1/\mu_0 = 0.25$ and figure (5b) shows the deflection for the hard coating $\mu_1/\mu_0 = 2$ subject to the different thicknesses $\hat{h} = 0.1, 0.5, 1$. These graphs show that the softer coating experiences a greater deflection than the harder coating which becomes more exaggerated as the thickness of the coating increases. Conversely, the harder coating experiences less deflection as coating thickness increases. These results are intuitively correct and serve as an initial check on the behaviour of the solutions given in this work.

5.2. Convergence study

In addition to determining an appropriate value of $\hat{L}$, we must determine a suitable value of N so as to ensure that our obtained solution is accurate. In order to do this, we consider plots of the

maximum amplitude of the coefficients P_n, U_n and V_n where

$$U_n = \sum_{j=1}^{4} A_j^{(n)}, \tag{73}$$

$$V_n = -\sum_{j=1}^{4} \gamma_{j,n} A_j^{(n)} \tag{74}$$

$n \in \mathbb{N}$ denote the maximum amplitude of the Fourier modes that comprise the horizontal and vertical deflection in the coating respectively. We note in this example that as $P_{2n} = 0$, all coefficients U_{2n} and V_{2n} will vanish as a consequence of (64a), (64b) and thus we plot $|P_{2n-1}|$, $|U_{2n-1}|$ and $|V_{2n-1}|$ here. These results are presented in figure (6). It is readily observed that the amplitude of the coefficients U_{2n-1} and V_{2n-1} die more quickly than the amplitude of P_{2n-1} as n becomes large. Whilst the magnitude of the coefficients U_{2n-1} and V_{2n-1} increases as $\hat{h}$ increases when n is small, the coating thickness does not change how quickly the amplitudes die. This allows us to conclude that if the chosen value of N is sufficiently large enough to ensure that the Fourier series representation of the pressure converges, both the horizontal and vertical displacements will also converge. Thus the subsurface stress field obtained will be accurate.

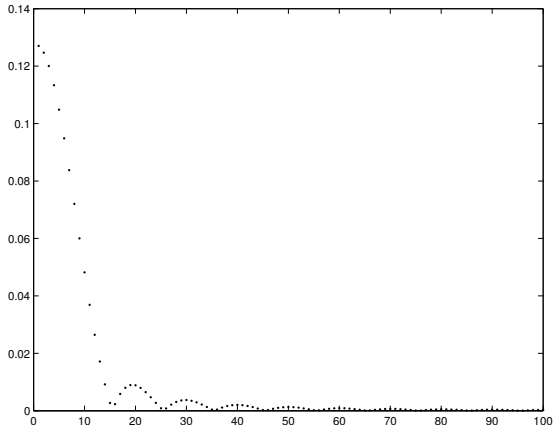

(a)

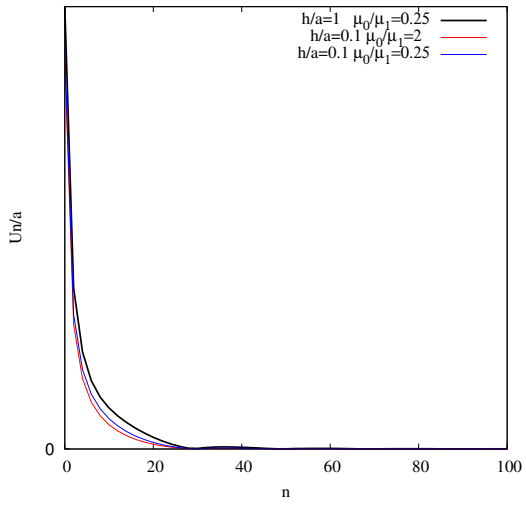

(b)

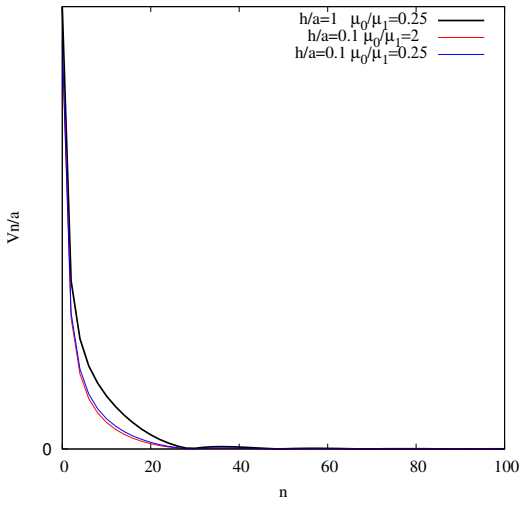

(c)

Figure 6: Plots of the magnitude of the coefficients a) P_{2n-1}, b) U_{2n-1} and c) V_{2n-1} for the values of $\hat{h}$ and μ_1/μ_0 given.

Table (1) details the maximum residual error in the Fourier representation of the pressure function using different values of N. It is seen that in order to obtain approximations that are accurate to within 1% of the true pressure, we must choose $N = 200$. Choosing $N = 400$ ensures that the maximum residual error is about 0.27% which is a reasonable improvement on the approximation returned with $N = 200$. A subsequent increase in the number of Fourier modes does not make

much difference to the maximum residual error and hence increases the computational expense of the approximation to the sub-surface stress field without providing much of an increase in accuracy. We therefore take $N = 400$ in this example.

The maximum residual error in Fourier approximations to the true pressure									
N	10	20	50	100	200	400	600	800	1000
RE	41%	17.71%	5.6%	2.47%	0.89%	0.27%	0.18%	0.137%	0.11%

Table 1: A comparison of the maximum residual error in the Fourier series approximation to the pressure function in example 1 using increasing numbers of modes.

5.3. Subsurface stress field

Figure (7) depicts the principal stress field (59) computed in the interval $-3 \leq X \leq 3, -2 \leq Y \leq 0$ for the soft coatings $\mu_1/\mu_0 = 0.25$ and 0.5. We are mainly interested in the effect of the coating thickness on the sub-surface stress field so we consider producing results for the three coating thicknesses $\hat{h} = 0.2, 0.5$ and 1.

It is immediately seen that the maximum principal stress is highly dependent on $\hat{h}$. Within thin layers, the maximum principal stress occurs in the substrate (figure (7a) and (7d), but steadily moves toward the interface as the layer becomes thicker (7b) and (7e) and finally transfers into the coating as the layer becomes thick (figures (7c) and (7f). It is also seen that a local island of high stresses could appear in the coating when the layer is thin (this will discussed in section 5.4).

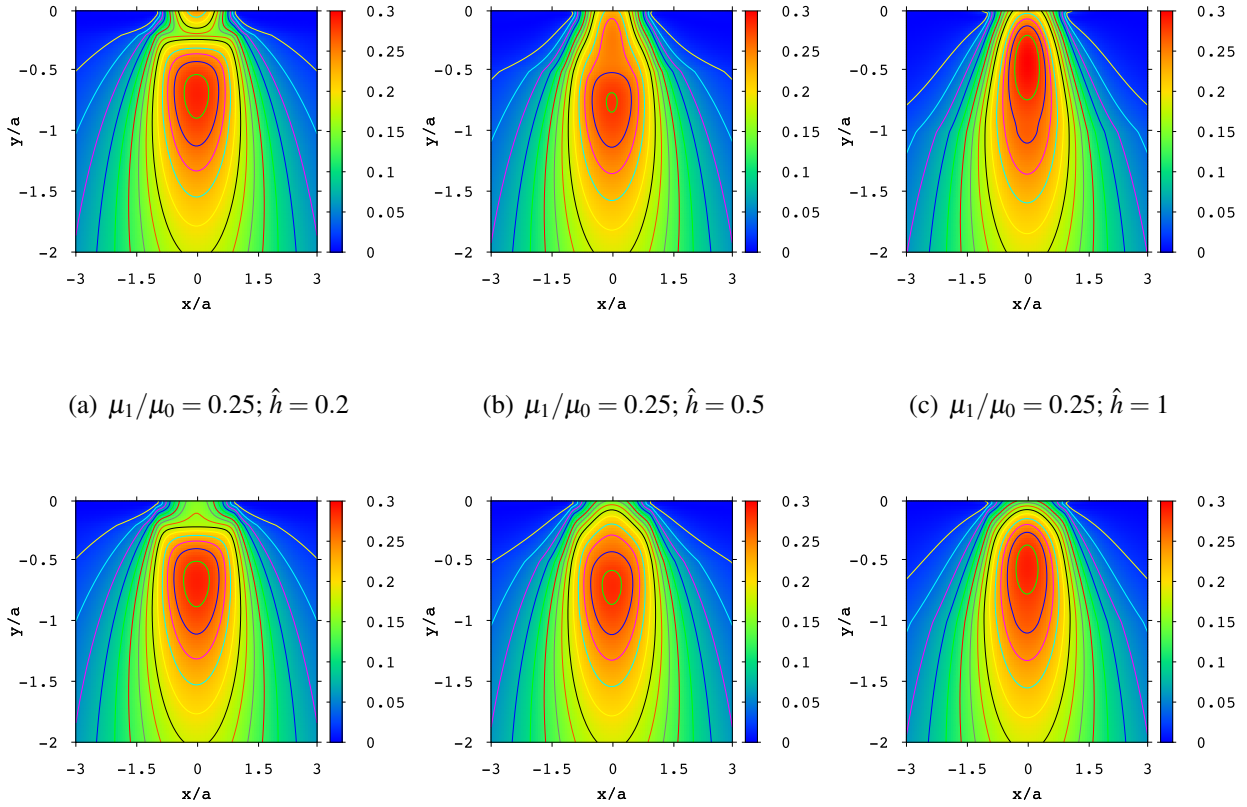

(a) $\mu_1/\mu_0 = 0.25; \hat{h} = 0.2$ (b) $\mu_1/\mu_0 = 0.25; \hat{h} = 0.5$ (c) $\mu_1/\mu_0 = 0.25; \hat{h} = 1$

(d) $\mu_1/\mu_0 = 0.5; \hat{h} = 0.2$ (e) $\mu_1/\mu_0 = 0.5; \hat{h} = 0.5$ (f) $\mu_1/\mu_0 = 0.5; \hat{h} = 1$

Figure 7: Contour plots of the sub-surface stress field for soft coatings that harden beneath the surface

The results presented in figure (8) for the hard coatings tend to follow the same general trend as those produced in figure (7) for soft coatings, but there are significant differences. In both cases, the maximum principal stress clearly transitions from the substrate into the coating as the coating progressively thickens. We note however that the magnitude of the maximum principal stress becomes larger as the coating thickness increases. This is in contrast to the results produced for the softer coating. Additionally, there seems to be a local island of very low stress within the coating very near the solid surface. This observation is very different to that made for the softer

coating.

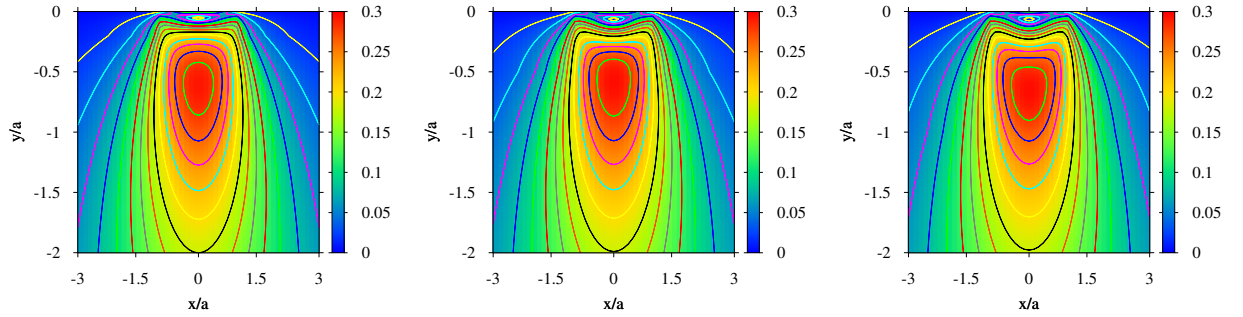

(a) $\mu_1/\mu_0 = 1.5; \hat{h} = 0.2$ (b) $\mu_1/\mu_0 = 1.5; \hat{h} = 0.5$ (c) $\mu_1/\mu_0 = 1.5; \hat{h} = 1$

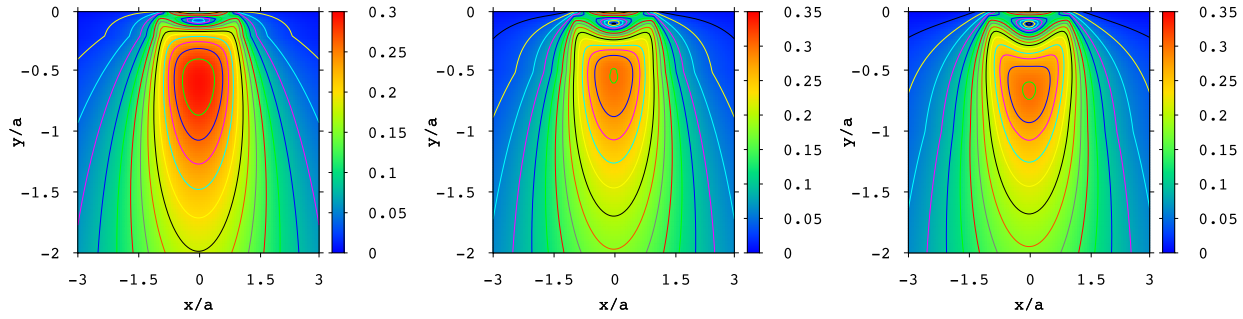

(d) $\mu_1/\mu_0 = 2; \hat{h} = 0.2$ (e) $\mu_1/\mu_0 = 2; \hat{h} = 0.5$ (f) $\mu_1/\mu_0 = 2; \hat{h} = 1$

Figure 8: Contour plots of the sub-surface stress field for hard coatings that soften beneath the surface

5.4. Determining the magnitude and location of the maximum principal stress

It was observed in figures (7) and (8) that the position of the maximum principal stress is highly dependent on the thickness of the coating. In order to investigate this phenomena more closely, we plot in figure (9) the local maxima $\max(\tau_1/p_0)$ within the substrate and coating together with the global maximum against $\hat{h} \in (0,1]$ for the case $\mu_1/\mu_0 = 0.25$. Additionally, we plot the depth at which the local maximum occurs within the coating and substrate. It should be noted in figure (9b)

that the diagonal line $y = -\hat{h}$ represents the coating-substrate interface.

It is seen that when the coating is very thin, the global maximum of τ_1/p_0 occurs within the substrate, whilst the local maximum within the coating occurs very close to the surface (figure (9b) and (10a)). As the coating begins to thicken, a small island emerges in the coating and the local maximum migrates below the surface (10a-b). In thicker coatings, this ridge expands and joins the region of high stress occuring in the substrate lying directly beneath the coating-substrate interface. Consequently, the local maximum in τ_1/p_0 occurs on the coating-subsurface interface (figure (10c). As the coating becomes thicker still, the global maximum value of τ_1/p_0 transfers into the coating and the local maximum principal stress within the substrate lies on the coating-substrate interface.

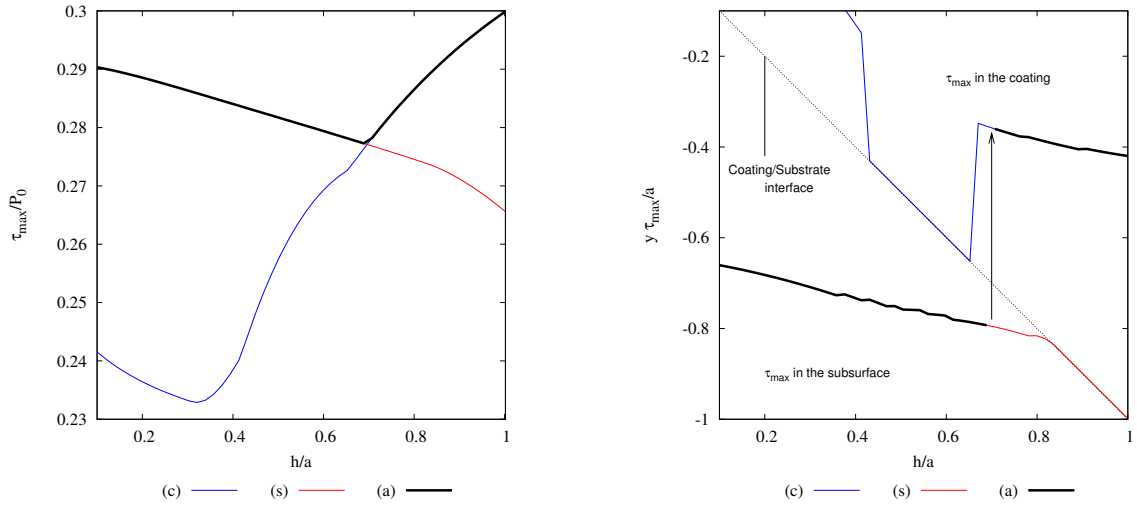

(a) Local and global maxima of (τ_1/p_0) (b) The position of the local and global maxima of (τ_1/p_0)

Figure 9: The behaviour of the maximum principal stress within the Coating (C), Substrate (S) and Global (G)

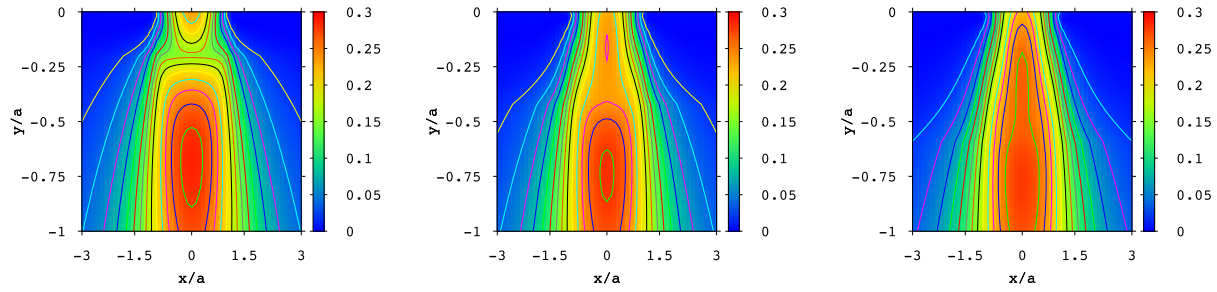

(a) $\hat{h} = 0.2$ (b) $\hat{h} = 0.42$ (c) $\hat{h} = 0.59$

Figure 10: Subsurface stress field $\mu_1/\mu_0 = 0.25$

The main goal of this paper is to propose a generic algorithm for determining the sub-surface stress field and localised deflection in a graded elastic bonded layered solid. However, this work can also provide a foundation for future failure mode prediction. Usually a hard material fails according to the Tresca criterion and a soft one according to the von Mises criterion. It is of particular interest in a practical problem to predict when the relevant criterion (depending on the problem) is met. As the coating and the substrate have different mechanical properties, it is possible that one of the materials will fail due to a local maximum in the stress field even if the global maximum occurs in the other region. Additionally, in many industrial applications, high stresses at the coating-substrate interface can induce local failure which will lead to exfoliation of the protective layer.

Figure (11) shows the global maximum of τ_1/p_0 and the location within the solid that it occurs for a variety of different coatings both hard and soft. It should be noted that both the magnitude of the global maximum of τ_1/p_0 and its position change significantly with layer thickness. Although there is always a noticeable change in the magnitude of the maximum stress when it migrates from

the substrate to the coating, this becomes more pronounced as the layer becomes softer. A similar trend is noted in the position of the maximum, as its jump in location from the substrate to the coating becomes sharper as the coating becomes softer.

The sudden jumps observed in the position of the maxima correspond to the layer thickness at which the local maxima within the coating overtake those in the substrate (see figure (7) and (8)). These results indicate that the mechanical properties of the coating/substrate must be optimised for each practical application in order to preserve the integrity of the system.

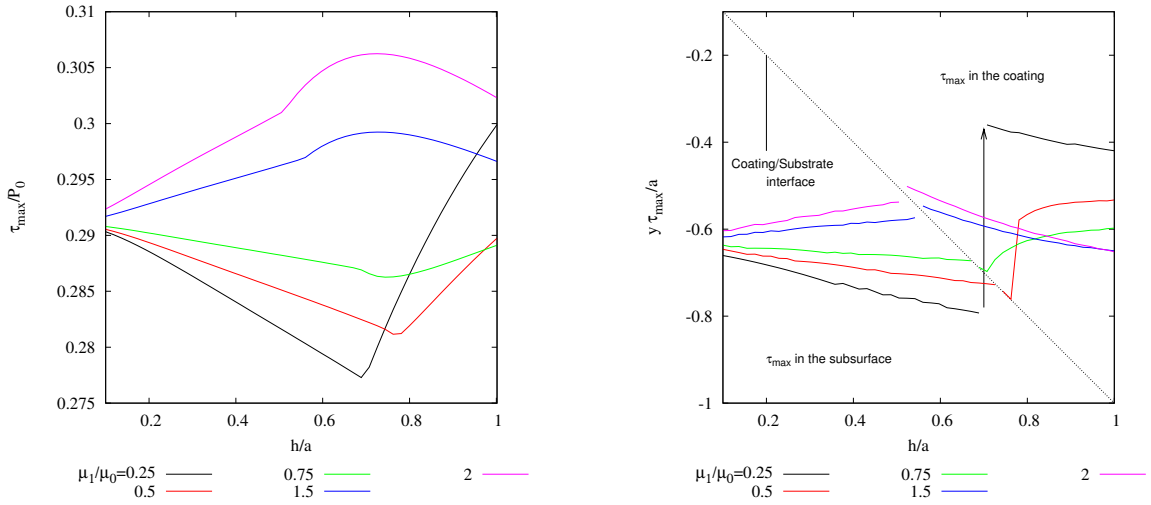

(a) Global maximum of (τ_1/p_0) (b) The position of the global maximum of (τ_1/p_0)

Figure 11: The behaviour of the maximum principal stress for a variety of coatings vs. $\hat{h}$

5.5. Comparison study

The solution propounded in this paper is valid only when the solid is inhomogeneously elastic. This is due to the necessity of having four distinct roots of (30) which is not the case if the solid is homogeneously elastic. There is however no restriction on the ratio μ_1/μ_0 as long as it is not

identically equal to one and thus we can take $\hat{\alpha}$ arbitrarily close to zero which corresponds to a solid which is almost homogeneous. It is then of interest to determine if a suitably small value of α can accurately model the stress field within a homogeneous solid.

In this example we choose

$$p(X) = p_0\sqrt{1-X^2} \tag{75}$$

which corresponds to the non-dimensional Hertzian pressure distribution and attempt to replicate the stress field computed using Hertzian theory (see Johnson (1985) for example) . The parameter values $\nu = 0.25$ and $N = 400$ remain fixed in this example whilst $\mu_1/\mu_0 = 1.1, 1.01, 0.9, 0.99, \hat{h} = 0.1, 1, 10$. Table (2) presents the maximum principal stresses max$)\tau_1/P_0$ (denoted$\tau_{\max}$) and the location that they are found ($Y_{\max}$) for these examples. It is found that all of the values of μ_1/μ_0 given above produce results that are in good agreement with those predicted by Hertzian theory ($\tau_{\max} = 0.3, Y_{\max} = -0.78$). The predicted maximum stresses are almost all within 1% of the predicted Hertzian maximum pressure. The only exceptions occur when $\mu_1/\mu_0 = 1.1$ and $\mu_1/\mu_0 = 0.9$ which is to be expected as these cases do not correspond to a solids which is almost homogeneous.

The depth at which the predicted values of max(τ_1/P_0) occur agree to within a 2% accuracy of the prediction obtained from Hertzian theory. In this case we see that the error in the approximation produced when $\mu_1/\mu_0 = 1.01$ and $\mu_1/\mu_0 = 0.99$ is 1.38%. However, as the error here becomes smaller as $|\alpha|$ decreases in magnitude, we conclude that in the limit $|\alpha| \to 0$, our model is capable of accurately modelling a homogeneously elastic solid. As a final check in this section, the principal stress field produced for this problem is depicted in figure (5.5) and is identical to the results presented by Johnson (1985).

The residual error in the predicted values of $\max(\tau_1/P_0)$ and the depth at which they occur				
μ_1/μ_0	Quantity	$\hat{h}=0.1$	$\hat{h}=1$	$\hat{h}=10$
$\mu_1/\mu_0=1.1$	$\tau_{\max}$	0.67%	1.23%	0.27%
	Y_{max}	1.13%	0.87%	2.15%
$\mu_1/\mu_0=1.01$	$\tau_{\max}$	0.63%	0.7%	0.7%
	Y_{max}	1.38%	1.38%	1.38%
$\mu_1/\mu_0=0.9$	$\tau_{\max}$	0.6%	0.02%	1.6%
	Y_{max}	1.9%	1.9%	0.62%
$\mu_1/\mu_0=0.99$	$\tau_{\max}$	0.63%	0.57%	0.73%
	Y_{max}	1.38%	1.38%	1.38%

Table 2: A comparison of the predicted maximum dimensionless principal stress for four solids that are almost homogeneously elastic subject to three different coating thicknesses.

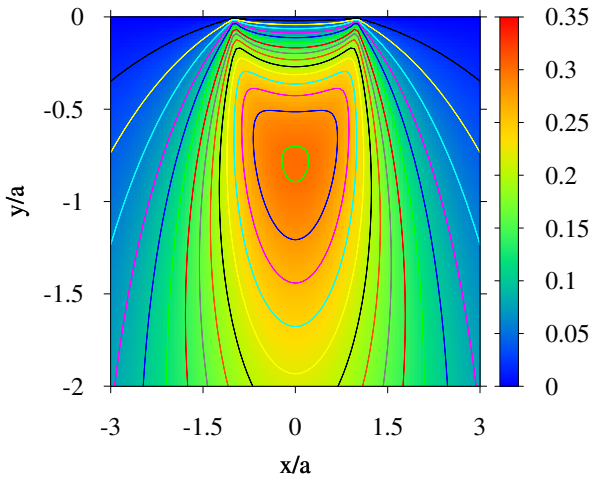

Figure 12: The stress field produced for the dimensionless Hertzian pressure given by

(75).

6. Conclusions

The derivation of a solution used to determine the stresses and deflection resulting from a contact problem is presented. The original problem is re-scaled and mapped to an alternate domain where the displacements within the problem prove receptive to solution by the separation of variables technique. As a result, the stresses and displacement within this problem may be represented in terms of Fourier series.

A simple surface pressure was considered within the confines of the contact problem to generate results using this model. A selection of coatings of different thicknesses and moduli of elasticity were considered and it was found that in general the thickness of the coating affects both the magnitude and position of the maximum principal stress within the solid. Further investigation

into this phenomena showed how the maximum principal stress induced by the applied surface pressure transitions from the substrate into the coating as coating thickness increases. This trend provides potentially valuable information in the manufacture of functionally graded materials.

The principal advantage of this method is that if the pressure applied in the contact problem is known, the solution detailed is analytic and requires no additional numerical calculations. This method is still valid for pressures that have been determined approximately but requires the numerical determination of the Fourier coefficients in the series expansion of the pressure. Overall, the computational expense using this model is kept to a minimum and provides fast yet accurate solutions to the contact problem.

Acknowledgement

The authors acknowledge the technical support from partners and sponsorship provided by the EPSRC through the ENCYCLOPAEDIC program grant.

References

Barbezat, G., 2008. Thermal spray applications in powertrain contribute to the saving of energy and material resources. Surface & Coatings Technology 202, 4428–4431.

Chidlow, S., Teodorescu, M., Vaughan, N.D., 2010. A new solution method for the contact mechanics of graded coatings. STLE/ASME International Joint Tribology Conference. October 17-20, San Francisco, California, USA .

Chidlow, S., Teodorescu, M., Vaughan, N.D., 2011. Determining the sub-surface stresses in a

graded-elastic solid using fourier series decomposition. 5th International Conference on Micro– and Nanosystems (MNS-1) IDETC2011. August 29-31, Washington, DC, USA .

Giannakopoulos, A.E., Suresh, S., 1997. Indentation of solids with gradients in elastic properties: Part 1. point force. Int. J. Solids Structures 34, 2357–2392.

Guler, M.A., Erdogan, F., 2004. Contact mechanics of graded coatings. Int. J. Solids Structures 41, 3865–3889.

Ke, L.L., Wang, Y.S., 2007. Two-dimensional sliding frictional contact of functionally graded materials. European Journal of Mechanics A/Solids 26, 171–188.

Sadd, M.H., 2010. Some simple cartesian solutions to plane non-homogeneous elasticity problems. Mechanics Research Communications 37, 22–27.

Shulha, H., Kovalev, A., Myshkin, N., Tsukruk, V.V., 2004. Some aspects of afm nanomechanical probing of surface polymer films. European Polymer Journal 40, 949–956.

Suli, E., Mayers, D.F., 2003. An introduction to Numerical Analysis. Cambridge University Press, Cambridge.

Suresh, S., Giannakopoulos, A.E., Padture, N.P., Jitcharoen, J., 1998. Functionally-graded materials. Speciffication, International application number PCT/US98/05188.

Suresh, S., Olsson, M., Giannakopoulos, A.E., Padture, N.P., Jitcharoen, J., 1999. Engineering the resistance to sliding-contact damage through controlled gradients in elastic properties at contact surfaces. Acta mater. 47, 3915–3926.

Teodorescu, M., Rahnejat, H., 2007. Mathematical modelling of layered contact mechanics of cam-tappet conjunction. Applied Mathematical Modelling 31, 2610–2627.

Teodorescu, M., Rahnejat, H., Gohar, R., Dowson, D., 2009. Harmonic decomposition analysis of contact mechanics of bonded layered elastic solids. Applied Mathematical Modelling 33, 467–485.

Timoshenko, S.P., Goodier, J.N., 1961. Theory of Elasticity. third ed. McGraw Hill Higher Education, New York.

Uozato, S., Nakata, K., Ushio, M., 2005. Evaluation of ferrous powder thermal spray coatings on diesel engine cylinder bores. Surface & Coatings Technology 200, 2580–2586.

Wang, Z.J., Wang, W.Z., Wang, H., Zhu, D., Hu, Y.Z., 2010. Partial slip contact analysis on three-dimensional elastic layered half space. Trans. ASME, J. Tribol. 132, 021403 (12 pages).

Zhong, Z., Shang, E., 2008. Closed-form solutions of three-dimensional functionally graded plates. Mechanics of Advanced Materials and Structures 15, 355–363.